Role of Feed-Forward Inhibition in Neocortical Information Processing: Implications for Neurological Disorders

Oleg V. Favorov, Olcay Kursun and Mark Tommerdahl

Department of Biomedical Engineering, University of North Carolina, Chapel Hill, NC 27599

Abstract

A major well-documented feature of cortical functional organization is the presence of prominent broadly tuned feed-forward inhibition in the input layer 4, in which local layer 4 inhibitory cells receive direct thalamocortical input and in turn suppress responses of neighboring layer 4 excitatory cells to their thalamocortical drive, thereby sharpening their receptive field properties. Here we review the evidence that the presence of broadly tuned feed-forward inhibition in layer 4 turns local layer 4 domains into functional analogs of Radial Basis Function networks, enabling layer 4 to contribute importantly to sensory information processing as a *pluripotent function linearizer*: i.e., it performs such a transform of afferent inputs to a cortical column that makes possible for neurons in the upper layers of the column to learn and perform their complex functions using primarily linear operations.

Feed-forward inhibition is subserved by fast-acting basket cells and slow-acting neurogliaform cells, which rely on $GABA_A$ and $GABA_B$ receptor-mediated inhibition, respectively. Their respective contributions can be observed by measuring tactile stimulus detection threshold using step vs. ramp vibrotactile stimuli. The static (step) threshold reflects basket-mediated inhibition, whereas the difference between the static and dynamic (ramp) thresholds reflects neurogliaform-mediated inhibition. Our feed-forward inhibition metric, which is based on the static and dynamic detection thresholds, can provide significant insight about the neurological health of the cortical circuitry, given that neurogliaform cells are engaged in on-demand energy homeostasis of cortical networks through their local release of insulin. For example, we have found this metric to be below normal in adolescents with autism spectrum disorder, but highly elevated in type 2 diabetes. Maladaptive feed-forward inhibition can have significant downstream implications for cortical information processing, and our metric can potentially be an effective means for evaluating a number of cortical abnormalities.

Contribution of Layer 4 to cortical information processing as a pluripotent function linearizer

Cortical areas comprising the neocortex are organized anatomically and functionally into multiple intertwined information-processing streams (Felleman and Van Essen 1991). These streams build their functional properties incrementally, with the hierarchically higher-level cortical areas

building their more complex functional properties on the simpler properties developed by the lower-level cortical areas (Iwamura 1998; Rauschecker 1998; Grill-Spector and Malach 2004). As a part of this functional elaboration, each successive cortical area receives its afferent input from the lower-level cortical areas and/or the thalamus and computes certain higher-order nonlinear functions over that input (Figure 1A). The computed nonlinear functions are not predefined, but are learned from experience (Sur and Rubenstein 2005).

In the field of machine learning and pattern recognition, it is well appreciated that learning nonlinear functions is much more difficult than learning linear functions. To overcome such difficulties, in 1990s a highly effective strategy emerged for dealing with nonlinear problems, according to which the problem's input space should be transformed into a new higher-dimensional "feature" space, in which the problem becomes linear and thus more readily solvable with efficient linear techniques (Schölkopf and Smola 2002). The proven success of this "problem-linearization" strategy in machine learning naturally raises a question whether such a strategy might also be used by neocortex in its experience-driven development, during which it acquires its unrivaled ability to recognize in its sensory input patterns the perceptually and behaviorally significant features of high degrees of nonlinear complexity and abstraction (Kourtzi and DiCarlo 2006; Freedman and Miller 2008).

All cortical areas face essentially the same task of learning to compute their nonlinear functions over their afferent inputs and all of them can benefit from doing their own function linearizations. The principal initial recipient of the afferent input to a cortical area is its Layer 4 (L4). L4 converts that input into a new form and outputs that new form to the upper layers (Layers 2 and 3, or L2/3) of the same cortical area for further processing (Figure 1B). The product of that L2/3 processing is then sent to L4 of the next cortical area, where the two-stage information processing operation is repeated (Figure 1A), but on a higher level, building on the advances made by the preceding cortical area (Rockland and Pandya 1979; Felleman and Van Essen 1991). The division of tasks between L4 and L2/3 does suggest that a function-linearization strategy might be implemented in L4 for the benefit of L2/3.

According to this strategy, the task of L4 cells would be to enable the L2/3 cells to learn and perform advanced nonlinear functions over the afferent inputs (i.e., their "target" functions) using fundamentally linear operations. This task is accomplished by transforming the afferent inputs in L4 in such a nonlinear manner that makes linear the relations between the outputs of the L4 cells and the target L2/3 functions. In their transformation of the afferent inputs, L4 cells in a cortical column will have to "linearize" target functions for the large number of cells comprising L2/3 of the column. Furthermore, since the L2/3 target functions are not specified *a priori*, but are developed by L2/3 cells gradually in a process of experience-driven self-organization and without providing any significant feedback to L4, the L4 cells will have to linearize the potential L2/3 target functions "blindly." This means that the L4 transform has to be "pluripotent." That is, the L4 transform should be optimized so as to make linear as broad a repertoire of potential functions over the afferent inputs as possible. The L2/3 cells will then select their target functions from this repertoire.

Although at a first glance such a pluripotent function linearization transform might seem daunting, its mathematically abstract elaboration under very basic cortically imposed constraints does readily

produce a computational system that closely resembles the real cortical L4 in its structure and functional properties (Favorov and Kursun 2011). Such a biologically realistic and highly effective pluripotent function linearizer has the following ingredients (Figure 2): (1) the output of each excitatory L4 cell is computed, in part, as a weighted sum of its afferent inputs, which are Hebbian; (2) lateral interconnections among L4 cells are used to diversify the afferent connectional patterns among L4 cells in a cortical column and give them a rich variety of receptive field properties; and (3) feed-forward inhibition makes L4 cells behave similarly to radial basis function (RBF) units and is principally responsible for function linearization capabilities. Importantly for the L4 linearizer's pluripotency, RBF networks are recognized as highly capable universal function approximators (Park and Sandberg 1991; Kůrková 2003).

Feed-forward inhibition is a prominent property of the real L4 functional architecture (Miller et al. 2001; Alonso and Swadlow 2005). Feed-forward inhibition of L4 excitatory cells (which include spiny stellates, pyramidal cells and star pyramids) is mediated by L4 inhibitory cells that are directly driven by the afferent inputs to the neighborhood (Porter et al. 2001; Hirsch et al. 2003; Swadlow 2003; Sun et al. 2006; Cruikshank et al. 2007; Hull et al. 2009). While this feed-forward inhibition is broadly tuned, comparable to the tuning of the afferent input, it effectively sharpens tuning of excitatory L4 cells by suppressing the weaker thalamic drive evoked by non-preferred stimuli (DeAngelis et al. 1992; Kyriazi et al. 1996; Bruno and Simons 2002; Swadlow 2002).

When the above computational model of L4 is developed on natural images and LGN-like input patterns and optimized for maximal pluripotency in linearizing arbitrary functions over natural images, it acquires structural and functional properties that closely match the properties of L4 of the cat primary visual cortex (Favorov and Kursun 2011). The list of nontrivial parallels, which are described in detail in Favorov and Kursun (2011), includes the following:

a) presence of inhibitory cells with strong direct thalamic inputs (Cruikshank et al. 2007) and unoriented RFs (Hirsh et al. 2003), which implement feed-forward inhibition;
b) high density of excitatory interconnections among the cells in the L4 network (Anderson et al., 1994; Tarczy-Hornoch et al. 1999);
c) anti-Hebbian plasticity of lateral excitatory connections among cells in the L4 network (Egger et al. 1999; Sáez and Friedlander 2009);
d) self-organization of LGN connections to L4 cells into narrow parallel ON-center and OFF-center strips, producing simple-cell receptive fields (Figure 3A; Hubel and Wiesel 1962; Alonso et al. 2001);
e) comparable numbers of receptive field subfields and aspect ratios (Jones and Palmer 1987; DeAngelis et al. 1993; Gardner et al. 1999);
f) emergence of end-inhibition receptive fields/hypercomplex cells (Figure 3A; Hubel and Wiesel 1962; Dreher 1972; Tolhurst and Thompson 1981);
g) prominent phase modulation of cells' responses to grating stimuli of optimal orientation (Figure 3B; Skottun et al. 1991);
h) narrow orientation tuning of comparable half-width at half-height (Figure 4; Rose and Blakemore 1974);
i) contrast invariance of orientation tuning (Figure 4; Sclar and Freeman 1982);
j) comparable average optimal spatial frequency of grating stimuli (Movshon et al. 1978);
k) narrower orientation tuning for grating stimuli of higher spatial frequencies (Vidyasagar and Siguenza 1985);

l) narrow orientation tuning of LGN inputs to L4 cells, close to orientation tuning of their outputs (Ferster et al. 1996; Chung and Ferster 1998);
m) presence of iso-orientation inhibition (Ferster 1986);
n) suppressive effects on cells' responses to optimally oriented grating stimuli by orthogonally oriented superimposed gratings (plaid-like stimuli; Bonds 1989; DeAngelis et al. 1992).

The presence of both feed-forward inhibition and anti-Hebbian lateral connections (which are unique to L4; see Egger et al. 1999; Sáez and Friedlander 2009) is required in order for L4 cells in the model to develop the biologically accurate diversity of multi-subfield receptive fields and acquire orientation tuning matching in sharpness that of real L4 neurons.

In conclusion, the fact that an efficient pluripotent function linearizer, designed on a few generic neurally-guided principles, exhibits emergent structural and functional properties that closely resemble those of cortical L4 strongly suggests that L4 has effective function-linearization capabilities and that its major function is to perform a transform of its afferent input enabling the upper layers to learn and compute complex functions using operations that are to a large degree linear.

Temporal stimulus-evoked dynamics of L4 feed-forward inhibition

Feed-forward inhibition in L4 is produced by basket cells and neurogliaform cells residing there. Both cell types receive strong afferent input, but basket cells act via fast $GABA_A$ receptor-mediated synaptic transmission, whereas neurogliaform cells release GABA as a volume transmitter and produce more slowly developing $GABA_A$ and very slow $GABA_B$ receptor-mediated inhibition (Tamas et al. 2003; Olah et al. 2009). As a result, feed-forward inhibition can be expected to have fast and slow temporal components, associated with basket and neurogliaform cells, respectively. This means that in response to a stimulus application, feed-forward inhibition in L4 develops gradually and, if the stimulus is continuing, feed-forward inhibition reaches its maximum a few hundreds of milliseconds after the stimulus onset. The initial – and only partial – stimulus-evoked feed-forward inhibition is generated exclusively by the basket cells, but then it is gradually augmented by the slowly developing contribution from the neurogliaform cells. Given our understanding (see above) that feed-forward inhibition contributes greatly to sharpening receptive field feature extracting properties of L4 cells (Figure 4), we can expect that the initial response of L4 cells to a stimulus will be less feature selective (and thus the stimulated individual less discriminative) than after a short period of continuing exposure to the stimulus.

Another aspect of somatosensation where fast vs. slow feed-forward inhibition should be clearly observable is in sensory testing of tactile stimulus detection threshold. The cells responsible for feed-forward inhibition are more responsive to weak afferent drive than are the excitatory L4 cells. Thus, sub-threshold or weak stimulus inputs should have the effect of raising the threshold at which excitatory L4 cells begin to respond to peripheral stimuli. Therefore, the sensory detection threshold should reflect the effectiveness of feed-forward inhibition: the stronger the feed-forward inhibition in a tested individual, the higher his/her detection threshold.

One sensory testing method that we have developed to examine feed-forward inhibition in human subjects involves the measurement of two independently collected values: (1) a "static" detection threshold, defined as the weakest 0.5s duration vibrotactile stimulus an individual can detect; and (2) a "dynamic" threshold, defined as the weakest slowly ramping vibrotactile stimulus an individual can detect (Figure 5). The **static threshold** is measured using a 20-trial Two Alternative Forced Choice (2AFC) Tracking protocol. During each trial a 25Hz vibrotactile test stimulus (lasting 500ms) is delivered to the tips of either index (D2) or middle (D3) fingers. Following each stimulus, the subject is prompted to select the skin site (D2 or D3) that was perceived to be stimulated. After a 5sec delay the stimulation is repeated until the completion of the 20 trials. The stimulus amplitude starts at 15μm and is modified based on the subject's response in the preceding trial. During the **dynamic threshold** protocol, a 25Hz vibrotactile stimulus is delivered to either D2 or D3. The amplitude of the stimulus starts from zero and is increased at a rate of 2μm/s. The subject is instructed to indicate the skin site receiving the stimulus as soon as the vibration is detected. Multiple trials are conducted and the results from those trials are averaged for each subject.

In our interpretation of these two tests, in the static threshold test the subject detects the presence of the threshold stimulus right at its onset, when feed-forward inhibition is coming only from fast basket cells but not from slow neurogliaform cells, allowing excitatory cells to respond with spike discharges to the stimulus-evoked afferent drive. In contrast, during the dynamic threshold test the stimulus starts at zero amplitude and grows in strength at a slow rate that is sufficient to engage slow-acting neurogliaform cells. By the time the stimulus amplitude reaches the static threshold (typically 4-5s into the stimulus), the feed-forward inhibition is stronger than during the static threshold test, coming now from both basket and neurogliaform cells, and it prevents excitatory cells from firing their spike discharges. Instead, the stimulus amplitude will have to be raised higher in order for the afferent drive to overcome feed-forward inhibition in the excitatory cells, so that they will finally emit spike discharges and evoke conscious perception of the stimulus. Computer simulation of this phenomenon is illustrated in Figure 6.

Consistent with this interpretation, dynamic thresholds have been demonstrated to be significantly elevated relative to static thresholds in healthy individuals across the age spectrum (Figure 7; Zhang et al. 2011). The plot in Figure 7 shows that although the static detection threshold rises with age (due to age-related changes in the skin), the dynamic threshold rises as well and continues to exceed the static threshold. This difference in the two measures can most parsimoniously be accounted for by feed-forward inhibition: i.e., the dynamic threshold is higher than the static threshold because the initial sub-threshold stimulus that is delivered during the dynamic testing increases the detectable threshold via feed-forward inhibition mediated by the neurogliaform cells.

Feed-forward inhibition in neurological disorders

Autism Spectrum Disorder. A number of populations with some type of neurological disorder have demonstrated a reduction in the difference between the static and dynamic thresholds. One of the most studied is autism spectrum disorder (ASD). Multiple lines of evidence point to GABA deficiencies as a problem in ASD (for review, see Purkayastha, et al. 2015 and Brondino et al.

2016) and it is clearly established that there is an imbalance in excitation and inhibition in this population. When measures of static and dynamic threshold were obtained in multiple studies in adolescents with ASD, there was little or no difference found between the two metrics, suggesting depressed neurogliaform cell-mediated feed-forward inhibition (Francisco et al. 2012; Puts et al. 2014, 2016; Tavassoli et al. 2015). Given the reliance of neurogliaform cells on $GABA_B$ receptor-mediated inhibition, this finding suggests that ASD might be associated in particular with reduced $GABA_B$ involvement in cortical operations.

In one of the studies (Puts et al. 2016), the same individuals with ASD who were found to have similar static and dynamic thresholds, were also found to have lower GABA levels based on their magnetic resonance spectroscopy (MRS) imaging. Figure 8 compares the test performance of 37 typically developing children (TDC) with 35 children with ASD studied by Puts et al. (2016). It shows no significant difference between static and dynamic thresholds in children with ASD, suggesting very little involvement of $GABA_B$ inhibition by neurogliaform cells in feed-forward inhibition. At the same time, the dynamic thresholds are very similar also between ASD and TDC groups (p = 0.55), indicating that their fully expressed feed-forward inhibition has comparable effectiveness. This indicates that $GABA_A$ inhibition by basket cells must be enhanced in the ASD group in order to compensate for the loss of $GABA_B$ inhibition. This inference is supported by the finding that $GABA_A$-specific static detection threshold in the ASD group is elevated relative to the TDC group (p = 0.03). The last inference to make from the collected data is that the reduced GABA levels in the ASD group, detected by MRS imaging, is likely to be due predominantly to reduction of GABA produced by neurogliaform cells.

Diabetes. Since we view depressed activity of neurogliaform cells as playing a major role in reducing dynamic detection threshold, we sought to study a population in which neurogliaform cells might be hyperactive. These cells happen to be the only known cells in the neocortex that produce and release insulin (Molnár et al. 2014). According to Csajbok and Tamas (2016), the function of neurogliaform cells is to regulate on-demand energy homeostasis of local cortical networks, and they respond to transient elevation of neural activity in local circuits during periods of information processing in three complementary ways. First, they release insulin, which increases transport of glucose into active neurons, thus satisfying their transient energy demands. Second, neurogliaform cell-released insulin suppresses excitation in cortical neurons. And third, neurogliaform cells release GABA, which also suppresses local neural activity via $GABA_B$ receptor-mediated inhibition. The second and third actions together curtail further energy demands of the local circuit.

In Type 2 Diabetes, insulin resistance impacts CNS and is associated with cognitive impairments (McNay and Recknagel 2011). We hypothesized that such insulin resistance in cortical networks could lead to chronic increase in insulin demand and consequently to hyperactivity in neurogliaform cells, which will manifest itself in elevated neurogliaform cell-mediated feed-forward inhibition. Based on this consideration, we measured static and dynamic detection thresholds in 37 Type 2 diabetic patients and found that the difference in dynamic and static thresholds in this group was significantly larger than in healthy control subjects (Figure 9). Even patients who were in the early stages of diabetes and had not yet developed peripheral neuropathy already had dynamic detection threshold statistically higher than the control population. Thus, this

sensory testing metric (i.e., the difference between the static and dynamic detection thresholds) could serve as a sensitive indicator of insulin resistance in neocortex and its impact on CNS information processing.

Could maladaptive feed-forward inhibition play a significant role in neurodegenerative processes? Cortical insulin is important for development of dendritic arbors and maintenance of excitatory and inhibitory synapses, thus contributing to the balance of excitation and inhibition in cortical networks (Csajbok and Tamas 2016). It is not inconceivable that altered activity of neurogliaform cells might play a role in the development of some neurodegenerative disorders, particularly those that have been linked with altered insulin activity. For example, a wide range of studies have implicated high levels of stress as playing a role in the development of PTSD (reviewed by Delaney 2010). Stress increases cortisol levels in the blood, which then damages brain cells by inhibiting insulin production, which leads to lower than normal glucose uptake. Thus, long-term stress leads to long-term metabolic problems in the CNS, which in turn results in a neuroinflammatory response. PTSD has been described in multiple studies as being the result of chronic neuroinflammation (Furtado and Katzman 2015). Additionally, there is a significant association of diabetes with PTSD (Egede and Dismuke 2012) and some success has been demonstrated with intranasal insulin treatment of acute psychological stress (Bohringer et al. 2008) as well as a variety of other neurocognitive disorders such as Alzheimer's disease (Chapman et al. 2013; de la Monte et al. 2013). Thus, there does appear to be some relationship between stress, CNS metabolism, neuroinflammation and insulin and the development of some neurodegenerative disorders.

It is also possible that local CNS insulin levels (which can be 10-100 times plasma insulin levels) play a role in the development of diabetes as a consequence of a neurodegenerative process. Impaired or excessive feed-forward inhibition mediated by neurogliaform cells could lead to altered CNS insulin levels, which would in turn modulate hypothalamic activity that has a downstream effect on pancreatic insulin production. In other words, impaired feed-forward inhibition, which would undoubtedly result in both sensory and cognitive deficits, and could be the result of an imbalance of excitation and inhibition, could lead to alterations in neurogliaform activity that impact CNS insulin levels.

Acknowledgements

Partial support for this work was provided by the Office of Naval Research, Applied Research Associates, and by TUBITAK-1001 Research Project (Project ID: 114E178).

References

Alonso JM, Swadlow HA (2005) Thalamocortical specificity and the synthesis of sensory cortical receptive fields. J Neurophysiol 94:26-32

Alonso JM, Usrey WM, Reid RC (2001) Rules of connectivity between geniculate cells and simple cells in cat primary visual cortex. J Neurosci 21:4002-4015

Anderson JC, Douglas RJ, Martin KAC et al (1994) Synaptic output of physiologically identified spiny stellate neurons in cat visual cortex. J Comp Neurol 341:16-24

Bohringer A, Schwabe L, Richter S et al (2008) Intranasal insulin attenuates the hypothalamic–pituitary–adrenal axis response to psychosocial stress. Psychoneuroendocrinology 33(10): 1394-1400

Bonds AB (1989) Role of inhibition in the specification of orientation selectivity of cells in the cat striate cortex. Vis Neurosci 2:41-55

Brondino N, Fusar-Poli L, Panisi C et al (2016) Pharmacological modulation of GABA function in autism spectrum disorders: A systemic review of human studies. J Autism Dev Disord 46(3):825-839

Bruno RM, Simons DJ (2002) Feedforward mechanisms of excitatory and inhibitory cortical receptive fields. J Neurosci 22:10966-10975

Chapman CD, Frey WH II, Craft S et al (2013) Intranasal treatment of central nervous system dysfunction in humans. Pharm Res 30(10): 2475-2484

Chung S, Ferster D (1998) Strength and orientation tuning of the thalamic input to simple cells revealed by electrically evoked cortical suppression. Neuron 20:1177-1189

Cruikshank SJ, Lewis TJ, Connors BW (2007) Synaptic basis for intense thalamocortical activation of feedforward inhibitory cells in neocortex. Nat Neurosci 10:462-468

Csajbok EA, Tamas G (2016) Cerebral cortex: a target and source of insulin? Diabetologia 59:1609-1615

DeAngelis GC, Robson JG, Ohzawa I et al (1992) The organization of suppression in receptive fields of neurons in the cat's visual cortex. J Neurophysiol 68:144-163

DeAngelis GC, Ohzawa I, Freeman RD (1993) Spatiotemporal organization of simple-cell receptive fields in the cat's striate cortex. I. General characteristics and postnatal development. J Neurophysiol 69:1091-1117

de la Monte SM (2013) Intranasal insulin therapy for cognitive impairment and neurodegeneration: current state of the art. Expert Opin Drug Deliv 10(12):1699-1709

Delaney E (2013) The relationship between traumatic stress, PTSD and cortisol. Naval Center for Combat & Operational Stress Control

Dreher B (1972) Hypercomplex cells in the cat's striate cortex. Invest Ophtalmol 11:355-356

Egede LE, Dismuke CE (2012) Serious psychological distress and diabetes: a review of the literature. Curr Psychiatry Rep 14(1):15-22

Egger V, Feldmeyer D, Sakmann B (1999) Coincidence detection and changes of synaptic efficacy in spiny stellate neurons in rat barrel cortex. Nature Neurosci 2:1098-1105

Favorov OV, Kursun O (2011) Neocortical layer 4 as a pluripotent function linearizer. J Neurophysiol 105: 1342-1360

Felleman DJ, Van Essen DC (1991) Distributed hierarchical processing in the primate cerebral cortex. Cereb Cortex 1:1-47

Ferster D (1986) Orientation selectivity of synaptic potentials in neurons of cat primary visual cortex. J Neurosci. 6:1284-1301.

Ferster D, Chung S, Wheat H (1996) Orientation selectivity of thalamic input to simple cells of cat visual cortex. Nature 380:249-252

Francisco E, Favorov O, Tommerdahl M (2013) The Role of Cortical Modularity in Tactile Information Processing: An Approach to Measuring Information Processing Deficits in Autism. In: Fitzgerald M (ed) Recent Advances in Autism Spectrum Disorders, vol II. InTech. doi:10.5772/54801.

Freedman DJ, Miller EK (2007) Neural mechanisms of visual categorization: insights from neurophysiology. Neurosci Biobehav Rev 32:311-329

Furtado M, Katzman MA (2015) Neuroinflammatory pathways in anxiety, posttraumatic stress, and obsessive compulsive disorders. Psychiatry Res 229(1): 37-48

Gardner JL, Anzai A, Ohzawa I et al (1999) Linear and nonlinear contributions to orientation tuning of simple cells in the cat's striate cortex. Vis Neurosci 16:1115-1121

Grill-Spector K, Malach R (2004) The human visual cortex. Annu Rev Neurosci 27:649-677

Hirsch JA, Martinez LM, Pillai C et al (2003) Functionally distinct inhibitory neurons at the first stage of visual cortical processing. Nature Neurosci 6:1300-1308

Hubel DH, Wiesel TN (1962) Receptive fields, binocular interactions and functional architecture in the cat's visual cortex. J Physiol (Lond) 160:106-154

Hull C, Isaacson JS, Scanziani M (2009) Postsynaptic mechanisms govern the differential excitation of cortical neurons by thalamic inputs. J Neurosci 29:9127-9136

Iwamura Y (1998) Hierarchical somatosensory processing. Curr Opin Neurobiol 8:522-528

Jones JP, Palmer LA (1987) The two-dimensional spatial structure of simple receptive fields in cat striate cortex. J Neurophysiol 58:1187-1211

Kyriazi H, Carvell GE, Brumberg JC et al (1996) Quantitative effects of GABA and bicuculline methiodide on receptive field properties of neurons in real and simulated whisker barrels. J Neurophysiol 75:547-560

Kourtzi Z, DiCarlo JJ (2006) Learning and neural plasticity in visual object recognition. Curr Opin Neurobiol 16:152-158

Kůrková V (2003) Universal approximators. In: Arbib MA (ed) The Handbook of Brain Theory and Neural Networks, 2nd edn. MIT Press, Cambridge, p 1180-1183.

McNay EC, Recknagel AK (2011) Brain insulin signaling: a key component of cognitive processes and a potential basis for cognitive impairment in type 2 diabetes. Neurobiology of Learning and Memory 96:432-442.

Miller KD, Pinto DJ, Simons DJ (2001) Processing in layer 4 of the neocortical circuit: new insights from visual and somatosensory cortex. Curr Opin Neurobiol 11:488-497

Molnár G, Faragó N, Kocsis Á et al (2014) GABAergic neurogliaform cells represent local sources of insulin in the cerebral cortex. J Neurosci 34(4):1133-1137.

Movshon JA, Thompson ID, Tolhurst DJ (1978) Spatial and temporal contrast sensitivity on neurons in areas 17 and 18 of the cat's visual cortex. J Physiol 283:101-120

Olah S, Fule M, Komlosi G et al (2009) Regulation of cortical microcircuits by unitary GABA-mediated volume transmission. Nature 461:1278-1282

Park J, Sandberg IW (1991) Universal approximation using radial-basis-function networks. Neural Comput 3:246-257

Porter JT, Johnson CK, Agmon A (2001) Diverse types of interneurons generate thalamus-evoked feed-forward inhibition in the mouse barrel cortex. J Neurosci 21:2699-2710

Purkayastha P, Malapati A, Yogeeswari P et al (2015) A review of GABA/glutamate pathway for therapeutic intervention of ASD and ADHD. Curr Med Chem 22(15):1850-1859

Puts N, Wodka E, Tommerdahl M et al (2014). Impaired tactile processing in children with Austism Spectrum Disorder. J Neurophysiol 111(9):1803-1811

Puts N, Wodka E, Harris A et al (2016) Reduced GABA and altered somatosensory function in children with Autism Spectrum Disorder. Autism Res. doi:10.1002/aur.1691

Rauschecker JP (1998) Cortical processing of complex sounds. Curr Opin Neurobiol 8:516-521

Rockland KS, Pandya DN (1979) Laminar origins and terminations of cortical connections of the occipital lobe in the rhesus monkey. Brain Res 179:3-20.

Rose D, Blakemore C (1974) An analysis of orientation selectivity in the cat's visual cortex. Exp Brain Res 20:1-17

Sáez I, Friedlander MJ (2009) Plasticity between neuronal pairs in Layer 4 of visual cortex varies with synapse state. J Neurosci 29:15286-15298

Schölkopf B, Smola AJ (2002) Learning with Kernels. MIT Press, Cambridge.

Sclar G, Freeman RD (1982) Orientation selectivity in the cat's striate cortex is invariant with stimulus contrast. Exp Brain Res 46:457-461

Skottun BC, Valois RL, Grosof DH et al (1991) Classifying simple and complex cells on the basis of response modulation. Vision Res 31:1079-1086

Sun QQ, Huguenard JR, Prince DA (2006) Barrel cortex microcircuits: thalamocortical feedforward inhibition in spiny stellate cells is mediated by a small number of fast-spiking interneurons. J Neurosci 26:1219-1230

Sur M, Rubenstein JLR (2005) Patterning and plasticity of the cerebral cortex. Science 310:805-810

Swadlow HA (2002) Thalamocortical control of feed-forward inhibition in awake somatosensory "barrel" cortex. Philos Trans R Soc Lond B Biol Sci 357:1717-1727

Swadlow HA (2003) Fast-spiking interneurons and feedforward inhibition in awake sensory neocortex. Cereb Cortex 13:25-32

Tamas G, Lorincz A, Simon A et al (2003) Identified sources and targets of slow inhibition in the neocortex. Science 299:1902-1905

Tarczy-Hornoch K, Martin KAC, Stratford KJ et al (1999) Intracortical excitation of spiny neurons in layer 4 of cat striate cortex *in vitro*. Cereb Cortex 9:833-843

Tavassoli T, Bellesheim K, Tommerdahl M et al (2015) Altered tactile processing in children with Autism Spectrum Disorder. Autism Res 9:616-620

Tolhurst DJ, Thompson ID (1981) On the variety of spatial frequency selectivities shown by neurons in area 17 of the cat. Proc R Soc Lond B 213:183-199

Vidyasagar TR, Siguenza JA (1985) Relationship between orientation tuning and spatial frequency of cat area 17. Exp Brain Res 57:628-631

Zhang Z, Francisco E, Holden J et al (2011) Somatosensory information processing in the aging population. Front Aging Neurosci 3:18. doi:10.3389/fnagi.2011.00018

FIGURE LEGENDS

FIGURE 1. Stages of cortical forward information processing. (**A**) Peripheral sensory input, delivered to the cortex via the thalamus, is passed through a series of cortical areas. Each area transforms its input from the preceding stage by computing a certain nonlinear output function F over it. This processing flow is illustrated on an example of the somatosensory cortex, comprising Brodmann cytoarchitectonic areas 3b, 1, 2, and 5, as well as somatosensory ventrobasal (VB) thalamic complex. (**B**) In each cortical area, the afferent input is first preprocessed in the input layer 4, which performs a function-linearization transform Φ, and then the output function F is computed in the upper cortical layers 2 and 3. The insert illustrates the function linearization strategy of transforming the input space into a "feature" space on an example of a classification problem. The curved decision boundary separating two classes of data samples (little red and blue squares) in the input space is made linear – and thus easier to learn – by mapping the data samples into a nonlinear transform of the input space.

FIGURE 2. Mathematical representation of the functional structure of macrocolumnar Layer 4 domains. Output of excitatory L4 cell *i* is computed as a function of its afferent inputs $a_1 \ldots a_n$ and lateral inputs from neighboring cells $\Phi_1 \ldots \Phi_k$; w_{ij} and ρ_{ik} are connection weights (Favorov and Kursun 2011).

FIGURE 3. The pluripotent function-linearizing L4 model, trained on natural images, develops receptive fields closely matching those of the simple cells in the visual cortex. (**A**) Two examples of simple-cell receptive fields and an end-stopping receptive field developed by the L4 model. (**B**) Single-cell property of prominent phase modulation of a model cell's response *F* to a moving grating stimulus at the optimal orientation vs. no response to the same grating at the orthogonal orientation.

FIGURE 4. Orientation tuning of the model L4 cells is contrast invariant and highly, but not fully, dependent on feed-forward inhibition. (**Left**) Average orientation tuning of all L4 cells with simple-cell receptive fields (gray curve – maximally contrasted grating stimuli; black curve – grating stimuli at 1/3 of the maximal contrast). Note that, just as in the real visual cortex, stimulus contrast does not change the tuning width. (**Right**) Average orientation tuning of all the simple cells with feed-forward inhibition turned off.

Figure 5. Sensory testing of human vibrotactile detection threshold. (**A**) Tactile stimulator. (**B**) Two vibrotactile detection thresholds are measured using static and dynamic threshold protocols.

FIGURE 6. Computer simulation of L4 response to static and dynamic threshold stimuli. The pluripotent function-linearizing model of a macrocolumnar L4 domain (Favorov and Kursun 2011) was used for simulation. The top plot shows the time-course of the mean L4 population firing rate during static (blue curve) and dynamic (red curve) sinusoidal skin stimulation. A hypothetical perceptual stimulus detection threshold is indicated by the green horizontal line. The bottom plot shows the time-course of the stimulating probe's skin indent. The step stimulation pattern (blue) evokes L4 response that barely exceeds the detection threshold and therefore its amplitude is taken as the static threshold. The ramp stimulation pattern (red) evokes a gradually rising L4 response, which crosses the detection threshold at a much higher stimulus amplitude, which is taken as the dynamic threshold.

FIGURE 7. Average vibrotactile detection thresholds measured in groups of healthy subjects of different ages using static and dynamic threshold protocols (Figure 5).

FIGURE 8. Average vibrotactile detection thresholds measured in 37 typically developing children and 35 children with ASD using static and dynamic threshold protocols (based on Puts et al. 2016).

FIGURE 9. Average vibrotactile detection thresholds measured in 17 healthy control subjects, 28 type 2 diabetes subjects without peripheral neuropathy, and 9 type 2 diabetes subjects with developed peripheral neuropathy using static and dynamic threshold protocols. Note that in the first two groups the static threshold is the same, but it is statistically higher in the third group, presumably due to their peripheral neuropathy.

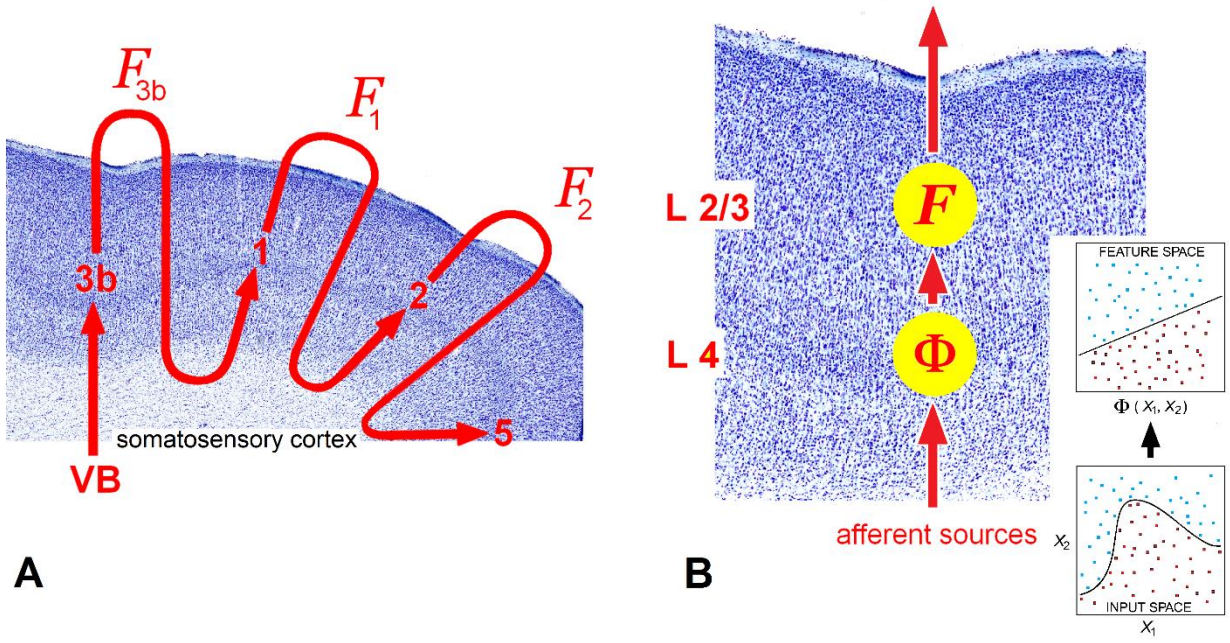
F_{3b}
F_1
F_2
3b
1
2
5
somatosensory cortex
VB
A
L 2/3
L 4
F
Φ
afferent sources
B
FEATURE SPACE
Φ (X_1, X_2)
X_2
INPUT SPACE
X_1

FIGURE 1

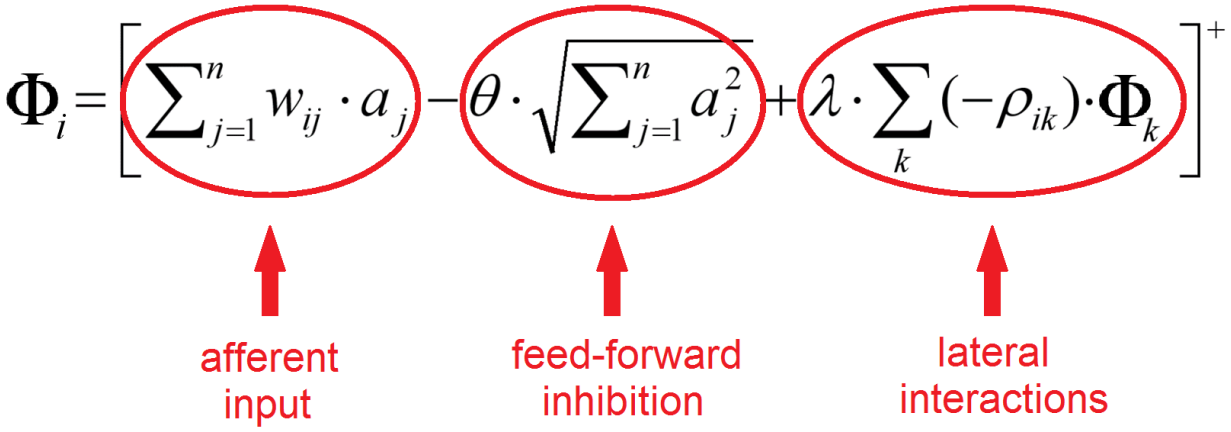
$\Phi_i = \left[\sum_{j=1}^{n} w_{ij} \cdot a_j - \theta \cdot \sqrt{\sum_{j=1}^{n} a_j^2} + \lambda \cdot \sum_k (-\rho_{ik}) \cdot \Phi_k \right]^+$
afferent input
feed-forward inhibition
lateral interactions

FIGURE 2

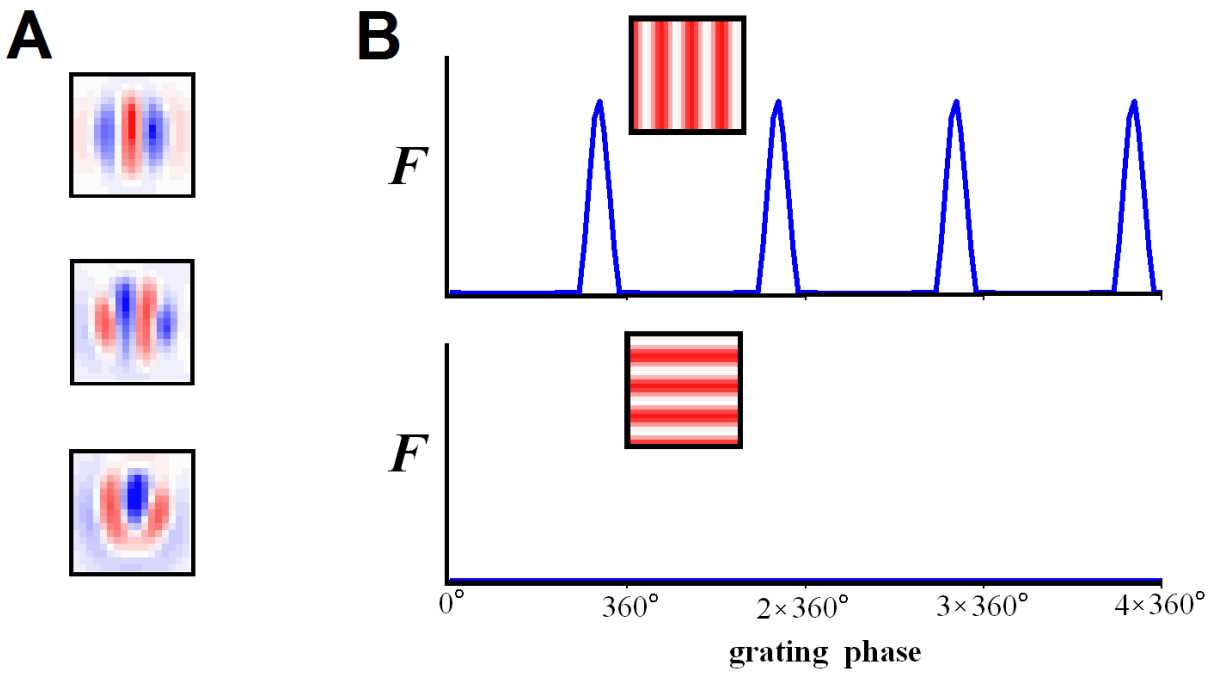

FIGURE 3

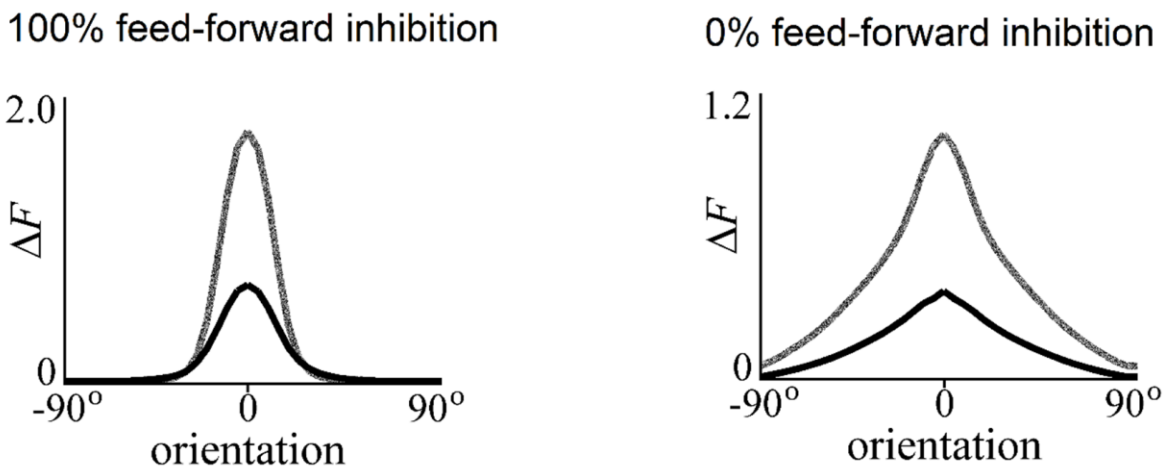
100% feed-forward inhibition
2.0
ΔF
0
-90°
0
90°
orientation
0% feed-forward inhibition
1.2
ΔF
0
-90°
0
90°
orientation

FIGURE 4

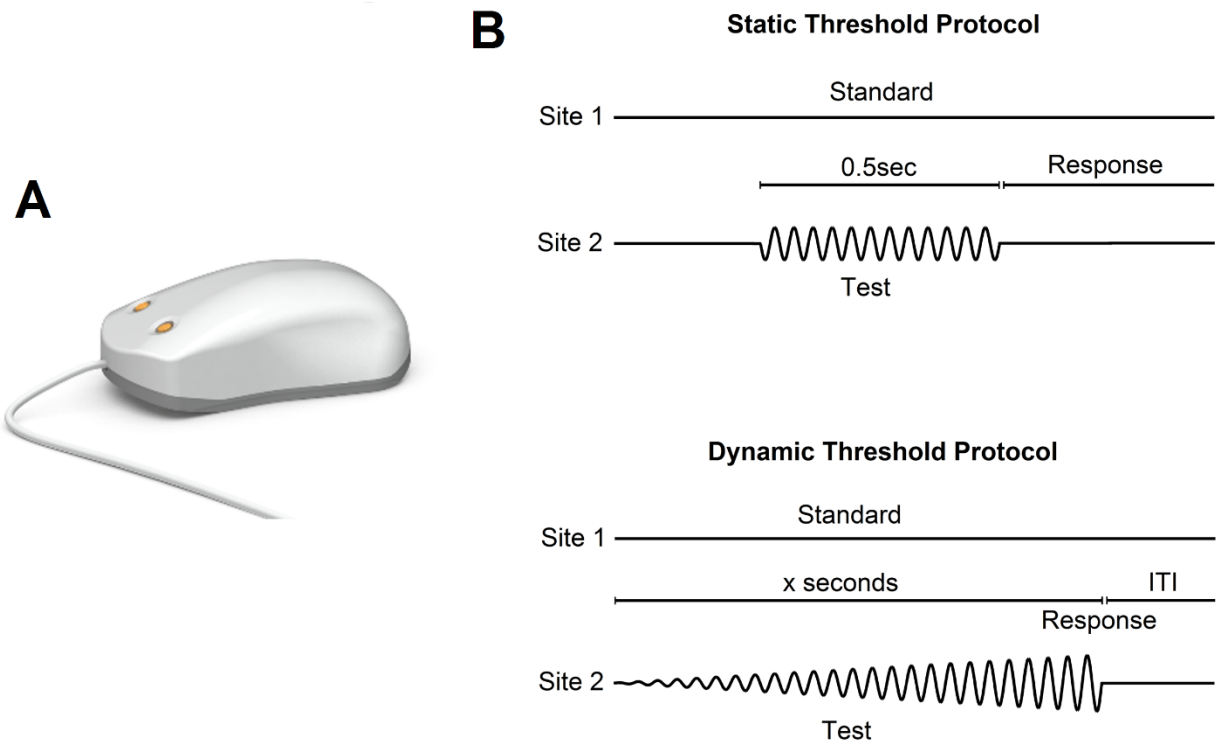
A
B
Static Threshold Protocol
Standard
Site 1
0.5sec
Response
Site 2
Test
Dynamic Threshold Protocol
Standard
Site 1
x seconds
ITI
Response
Site 2
Test

FIGURE 5

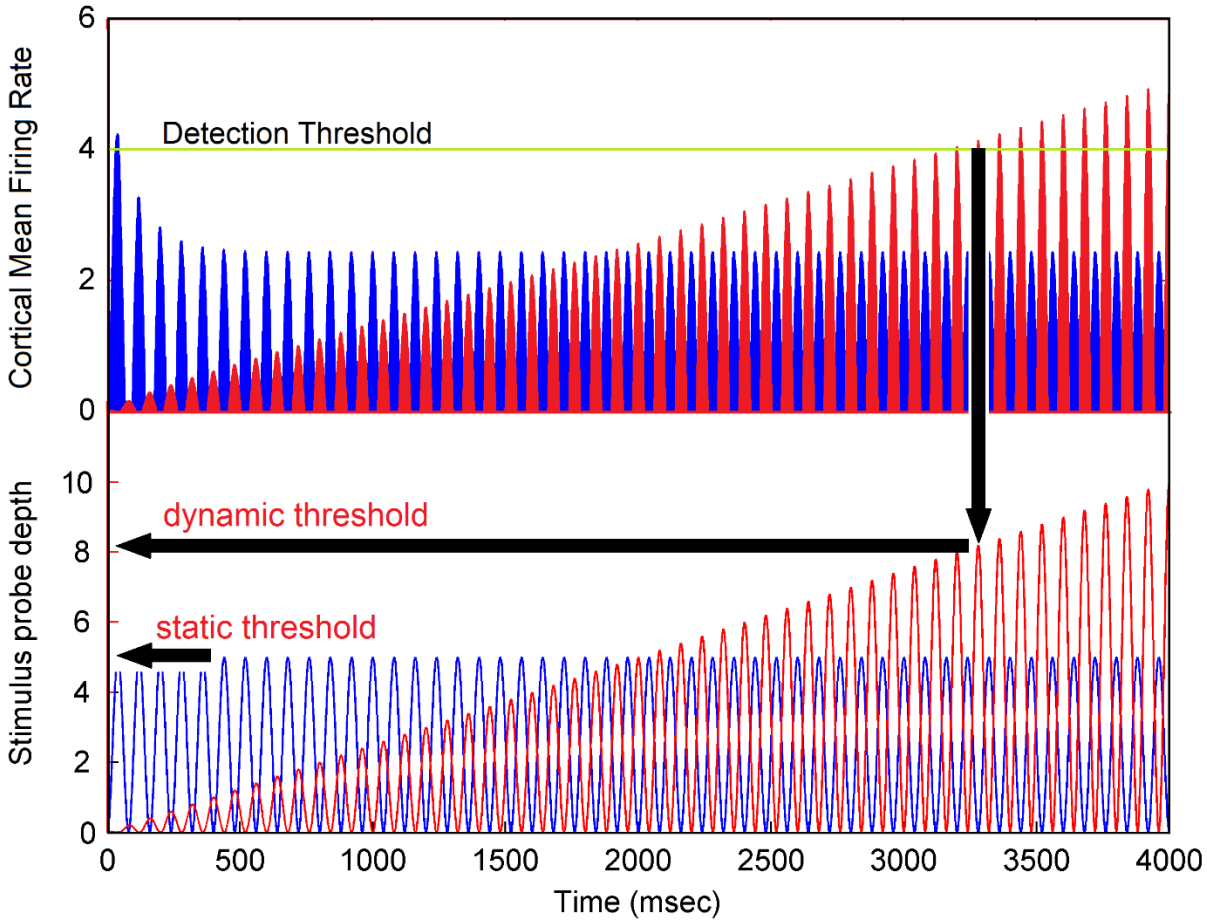
Cortical Mean Firing Rate
6
4
2
0
Detection Threshold
Stimulus probe depth
10
8
6
4
2
0
dynamic threshold
static threshold
0
500
1000
1500
2000
2500
3000
3500
4000
Time (msec)

FIGURE 6

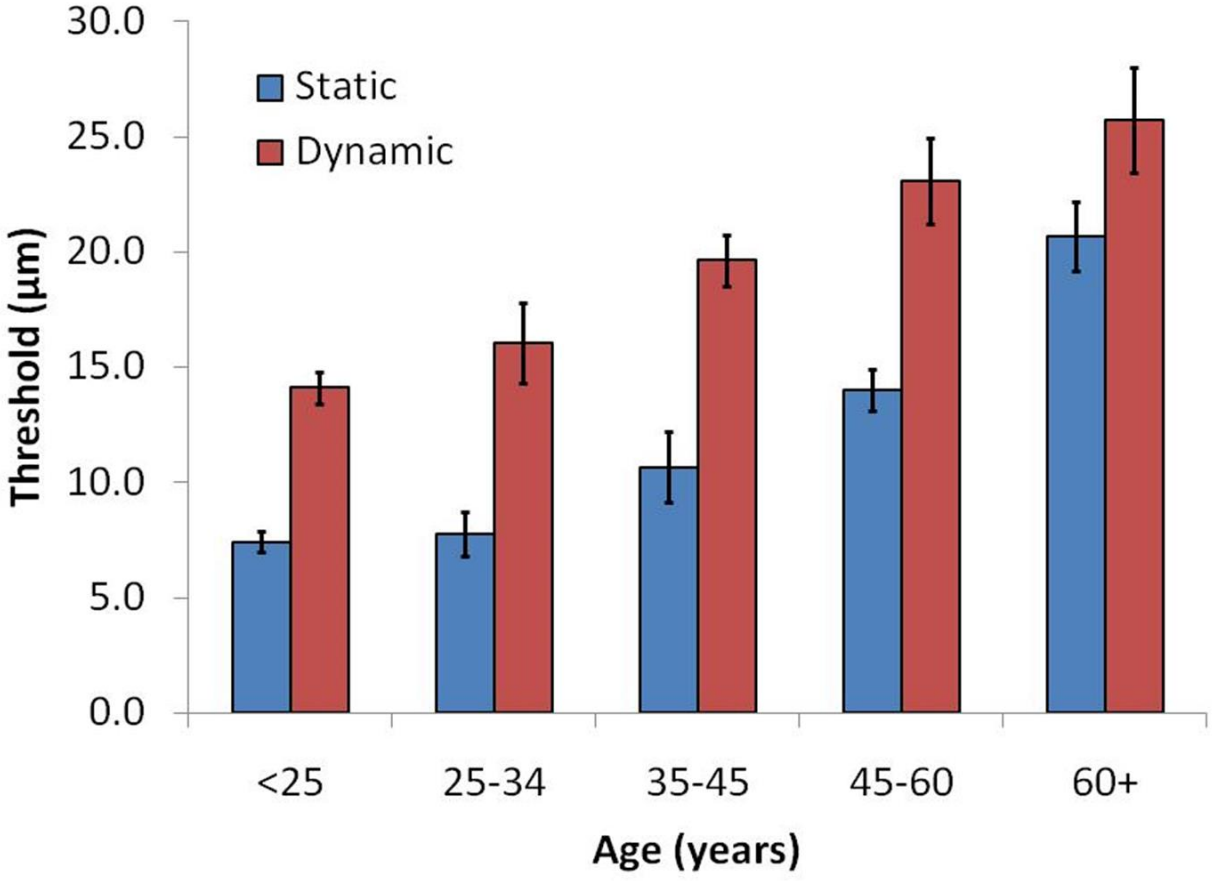
30.0
25.0
20.0
15.0
10.0
5.0
0.0
Threshold (µm)
Static
Dynamic
<25
25-34
35-45
45-60
60+
Age (years)

FIGURE 7

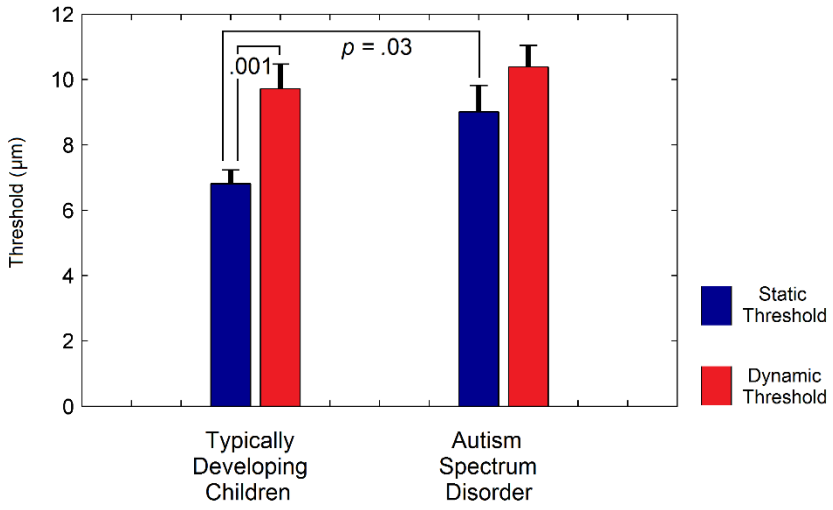
12
10
8
6
4
2
0
Threshold (μm)
p = .03
.001
Typically Developing Children
Autism Spectrum Disorder
Static Threshold
Dynamic Threshold

FIGURE 8

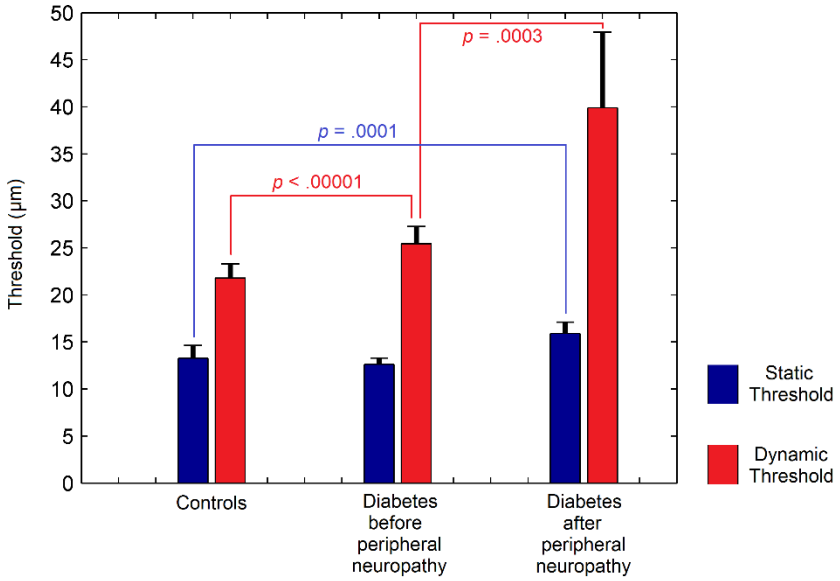
50
45
40
35
30
25
20
15
10
5
0
Threshold (µm)
p = .0003
p = .0001
p < .00001
Controls
Diabetes before peripheral neuropathy
Diabetes after peripheral neuropathy
Static Threshold
Dynamic Threshold

FIGURE 9